



Observation of Gigawatt-Class THz Pulses from a Compact Laser-Driven Particle Accelerator

A. Gopal,^{1,2,*} S. Herzer,^{1,2} A. Schmidt,¹ P. Singh,^{1,†} A. Reinhard,¹ W. Ziegler,¹ D. Brömmel,³ A. Karmakar,^{3,‡}
P. Gibbon,³ U. Dillner,⁴ T. May,⁴ H-G. Meyer,⁴ and G. G. Paulus^{1,2}

¹*Institute of Optics and Quantumelectronics, Friedrich-Schiller-Universität Jena, Max-Wien-Platz 1, 07743 Jena, Germany*

²*Helmholtz Institute Jena, Fröbelstieg 3, 07743 Jena, Germany*

³*Forschungszentrum Jülich GmbH, Institute for Advanced Simulation, Jülich Supercomputing Centre, D-52425 Jülich, Germany*

⁴*Institut für Photonische Technologien, Postfach 100239, 07702 Jena, Germany*

(Received 10 December 2012; published 15 August 2013)

We report the observation of subpicosecond terahertz (*T*-ray) pulses with energies $\geq 460 \mu\text{J}$ from a laser-driven ion accelerator, thus rendering the peak power of the source higher even than that of state-of-the-art synchrotrons. Experiments were performed with intense laser pulses (up to $5 \times 10^{19} \text{ W/cm}^2$) to irradiate thin metal foil targets. Ion spectra measured simultaneously showed a square law dependence of the *T*-ray yield on particle number. Two-dimensional particle-in-cell simulations show the presence of transient currents at the target rear surface which could be responsible for the strong *T*-ray emission.

DOI: [10.1103/PhysRevLett.111.074802](https://doi.org/10.1103/PhysRevLett.111.074802)

PACS numbers: 41.75.Jv, 52.25.Os, 52.59.Ye

Terahertz (*T*-ray) sources are considered to be next-generation light sources with applications ranging from cancer diagnosis to material science [1–5]. Due to their nonionizing nature, good spatial resolution, and the ability to penetrate several millimeters of biological tissue, *T* rays are a suitable alternative to x rays for the detection of cancerous cells [6]. Apart from biological imaging, powerful *T* rays find many applications in diagnostic tools for material science, such as ultrafast spectroscopy [7]. By focusing high power *T* rays to millimeter spot size, electric fields of the order of GV/m can be generated. Such large electric fields can be used to study structural transitions in polar molecules. The associated transient magnetic fields (of the order of a tesla) can be employed to create magnetic or spin excitations and to follow their dynamics on a picosecond time scale [8,9]. Currently available sources of high power *T* rays range from large scale facilities like linear accelerators [10] to compact sources based on electro-optic crystals [11]. Linear accelerators send a beam of relativistic electron bunches through a bending magnet to generate THz beams with megawatt (MW) peak power [12]. Sources based on electro-optic crystals use high repetition rate laser systems for generating *T* rays by optical rectification (OR) in nonlinear crystals. Both sources have advantages and disadvantages. For instance, *T*-ray sources based on accelerators are high peak power (MW), high repetition rate systems. However, they are large and expensive and thus can offer only fairly limited accessibility. Compact sources based on OR are more economic and can achieve *T*-ray pulses with energies comparable to accelerator based sources [13]. However, the *T*-ray yield is limited by the damage threshold of the nonlinear crystals. Such limitations do not exist for laser-generated plasmas. Accordingly, the potential of laser plasmas has been the subject of research since quite some time. In fact, there are various mechanisms by which the *T* rays are generated [14–20]. For plasma

filaments produced by two-color lasers, *T*-ray energy as high as $5 \mu\text{J}$ with a conversion efficiency of 1×10^{-4} was achieved [16]. However, at higher laser intensities, the THz radiation is subject to saturation due to intensity clamping [21], low electron density, and reabsorption of the radiation [16,22]. Plasmas generated during high-power laser-solid interaction do not have such limitations and are also a known source of *T* rays [17,18], however much less investigated.

In this Letter, we report the experimental observation of extremely powerful *T* rays from a laser-driven ion accelerator at incident laser intensities $>10^{19} \text{ W/cm}^2$. We measured subpicosecond pulses with energies $\geq 460 \mu\text{J}$ and a conversion efficiency $>7 \times 10^{-4}$, which is significantly higher than previously reported measurements [23]. *T* rays were emitted from the rear surface of a solid target in the noncollinear direction and we characterized the spectrum from 0.1–30 THz.

The experiment was performed at the multi-Terawatt JETI (Jena Ti-Sapphire) laser at the University of Jena [24]. The experimental configuration is similar to the one used in our previous measurements [23]. For this experiment the temporal contrast of the laser pulse was optimized to generate peak proton energies of 4.7 MeV with $5 \mu\text{m}$ thick titanium foils. Additionally, high transmission broadband THz windows (TPX $\leq 10 \text{ THz}$ or KRS-5 $\geq 8 \text{ THz}$) were used to couple the beam out of the experimental chamber. Simultaneous recording of the THz signal and the ion spectra allowed us to estimate the correlation between the THz power and the particle number.

By careful calibration of all the optical components in the beam path, a lower bound for the total energy of the emitted *T* rays was determined. For incident laser energies of 600 mJ, we measured *T*-ray pulses of at least $460 \mu\text{J}$ in the 0.1–30 THz band from a $5 \mu\text{m}$ thick titanium foil, which corresponds to a conversion efficiency of $>7 \times 10^{-4}$.

We emphasize that this value should be understood as the minimum conversion efficiency; losses occurring in the coupling of the T -ray beam to the detector outside the vacuum chamber are not taken into account. The geometry of the collection optics and the beam relay system ensured that only radiation emitted in the noncollinear direction was detected. The simultaneous recording of the ion spectra (Fig. 1 inset) showed typical thermal energy distributions [25] with peak proton energies up to 4.7 MeV. When the thickness of the target was varied from 2 to 10 microns, the total T -ray energy along with the peak proton energy and number decreased. Additional polarization measurements (using wire grid polarizers) showed that the THz emission is either radially polarized or unpolarized. Accordingly, the signal strength was reduced to half when a linear polarizer was inserted, irrespective of its orientation.

The temporal shape of the T -ray pulse was measured using a single-shot noncollinear pump-probe technique based on the electro-optic effect [26] in a gallium phosphide (GaP) crystal. In this scheme, the optical probe pulse and the THz pulse enter the electro-optical crystal at an angle; hence, there is a temporal skew in the probe wave front with respect to the THz wave front. The THz electric field induces birefringence proportional to the field strength in the crystal, which modulates the polarization of the optical probe. This modulation was analyzed using a prism polarizer and a CCD camera.

The data show that most of the energy is concentrated in a peak of ≈ 570 fs (FWHM) duration which indicates that peak powers close to a gigawatt can be attained. The polarizer angle was varied and the birefringence was measured which allowed us to estimate the induced ellipticity on the linearly polarized optical probe pulse by the THz field in the GaP crystal. Figure 2(a) shows the recorded

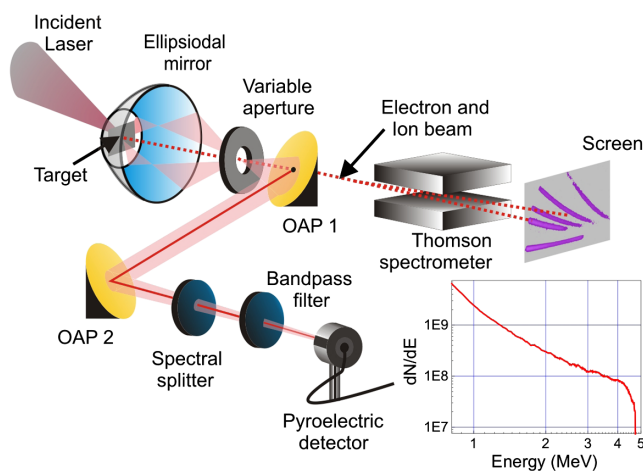


FIG. 1 (color online). Experimental scheme. The laser beam was focused onto a thin metal foil placed at the first focus of the ellipsoidal collection optics. T rays emitted in noncollinear directions are focused at the second focus of the ellipse. Inset shows a typical proton spectrum.

THz electric field after correcting for the background inhomogeneity of the optical probe beam. From the induced birefringence of the optical probe beam, we can infer a peak THz field of the order of 0.2 GV/m in the GaP crystal. Taking into account the THz beam diameter at the crystal and the measured pulse duration, a THz pulse of 200 μ J is detected below 10 THz which fits well with the actual energy measured in this spectral range using the pyroelectric detector. Figure 2(b) presents the corresponding spectral distribution. The blue solid curve represents the power spectral density obtained from the pump-probe measurement. Since the precision of the electro-optic measurements decreased in the high frequency region, additional spectral measurements were carried out using a set of well-defined band pass filters placed in front of the detector. The analysis presented in Fig. 2(b) (red dashed curve) shows a broad distribution of frequencies ranging from 0.3 to 30 THz. The two independent measurements show that most of the energy is distributed in the low frequency region even though the emission extends up to 30 THz. The high noise level in the electro-optical measurements (blue solid curve) is due to the low transmission of frequencies above 3 THz through the vacuum window (above 1.5 THz, the transmission was below 40%) and air. In other words, the spectral components above 3 THz that arrived at the crystal were much weaker than the signal generated inside the vacuum chamber. Therefore, we see a noisy signal beyond 3 THz using pump-probe diagnostics. Despite these limitations, the slopes of the spectral density curves are comparable using two independent measurement techniques.

Various physical models have been proposed for the generation of terahertz radiation from solid density plasmas. For the emission from the front side of the target, the antenna mechanism [18] and the current arising from the longitudinal ponderomotive force of the laser pulse [17] have been held responsible. Since the T rays emitted from the rear surface are highly noncollinear and the laser pulse incident on the front surface does not travel to the rear surface, the above mechanisms cannot account for the strong noncollinear emission from the rear surface. In our previous work [23], we proposed that the sheath

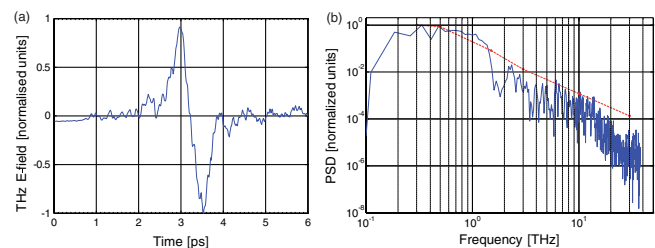


FIG. 2 (color online). Results of pump probe measurements. (a) Electric field of the THz pulse obtained from the pump-probe measurement. (b) Power spectral density obtained from the electro-optic measurement (blue solid curve) and using a set of calibrated bandpass filters (red dashed curve).

acceleration process at the target rear surface may be responsible for the strong noncollinear emission. Although this generation mechanism of T rays is complex, it can be understood in a simplified model based on the target normal sheath acceleration (TNSA) [25] as follows. The spatiotemporal charge distribution in the electrostatic sheath formed at the target rear surface during high-power laser-solid interaction can also be considered as an accelerating dipole. Because of the transient nature of this electrostatic sheath field, emission of radiation in the THz frequency band is expected. The direction of the emission is perpendicular to the direction of acceleration in the nonrelativistic regime. The power of the radiation emitted by the particles is given by the Larmor formula [27], $P = 2/3c^3 \ddot{d}^2$, where $\ddot{d} = \sum e \ddot{x}$; i.e., the power of the emitted radiation is proportional to the square of the number of the particles and their magnitude of acceleration which in turn is directly proportional to the strength of the electrostatic sheath field. Both parameters can be determined from the particle spectra recorded by the ion spectrometer.

To verify this, we simultaneously recorded the THz signal and the ion spectra for every shot. The incident laser intensity on target was varied from $(1-6) \times 10^{19}$ W/cm² by varying the laser energy. Therefore, we could vary the peak proton energy and the particle number. The number density and energy of various ion species and protons were extracted from the particle spectra. The maximum proton energy increased from 2.9 to 4.7 MeV. Proton counts increased following a power law with an exponent 0.76, while the T -ray signal followed a steeper power law with an exponent of 1.47 (not shown here). Figure 3 presents the T -ray yield as a function of detected proton counts and the correlation between the T -ray yield and the particle number shows a power law exponent of 1.76 ± 0.49 and is in agreement with our model, implying a dipolelike emission at the target rear surface.

As mentioned earlier, the current measurements report significantly higher T -ray yield compared to previous observations [23]. This improvement can be accounted for by a combination of better temporal contrast of the

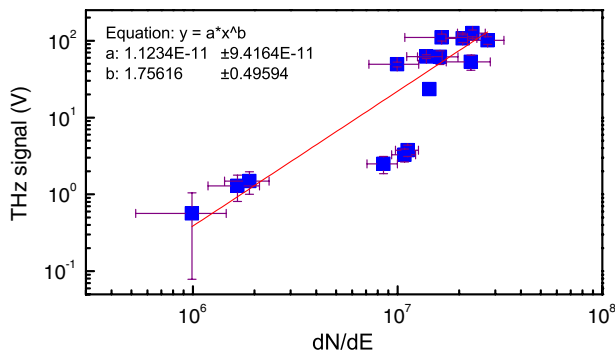


FIG. 3 (color online). T -ray yield as a function of the number of protons measured in a 50 keV energy interval per $10 \mu\text{sr}$. Error bars indicate the shot-to-shot fluctuation.

laser pulse and more favorable target configuration, leading to stronger TNSA both in higher particle numbers ($10\times$) and energies ($1.4\times$) compared to Ref. [23], which given the above scaling, accounts for much of the $200\times$ higher THz energy yield observed in the current experiment. Moreover, we have determined that the T -ray emission in the forward direction (target normal direction) is 2 orders of magnitude smaller than the noncollinear emission, implying that the contribution from the recirculating electrons is insignificant.

To estimate the total T -ray yield, the ion numbers and acceleration of each species (calculated from their energies) can be substituted in the Larmor formula above, giving an output power of 3.5 ± 1 MW. However, the particle spectra are measured over a $10 \mu\text{sr}$ solid angle, much lower than the 23msr emission angle previously measured under similar conditions [24]. Correcting for this selectivity results in an estimated power $O(1)$ GW, which is consistent with the THz energies detected using the pump-probe measurements. Moreover previous simulations [28] suggest more than 1% energy conversion into ions at these intensities, or at least 6 mJ, which over the longer ion acceleration time scales (~ 100 fs) gives 60 GW. Hence a conversion efficiency of 1% (from accelerated particles to THz) would also lead to terahertz radiation with GW power.

A series of 2D simulations were performed to gain more insight into the physics of T -ray emission using the particle-in-cell code JUPIC [29] on the JUROPA cluster at the Jülich Supercomputing Centre. Details of the simulation set up are given in the Supplemental Material [30]. The results of this simulation are presented in Fig. 4. Figure 4(a), shows the time trace of the THz radiation (Poynting vector) on the observation semicircle ($r = 20 \mu\text{m}$). A time gated polar plot of the THz radiation (60 ± 30 THz) for various semicircles (20, 40, and $60 \mu\text{m}$) is shown in Fig. 4(b) revealing a directionality consistent with the experimental observations. To understand the source of the THz emission, the current and particle distribution along and perpendicular to the target rear surface were plotted. Analysis of these quantities shows that the origin of these high-frequency T rays is a transient. Initially ($t \approx 160$ fs), electrons pass through the foil and fan out in a cloud on the rear side. The deficit of negative charge on the laser axis draws a return current along the rear surface, which eventually reverses—Fig. 4(c). This effectively creates a diametrically opposed pair of currents either side of the laser axis (in 3D this would be a radial current), with a lifetime of 100–150 fs depending on the distance from the axis [Fig. 4(e)]. The resulting radiation field emitted by this current is shown in Fig. 4(a), where the time delay between the $J_{y\text{min}}$ in (c) at 180–200 fs and the peak field between 300 and 350 fs matches the time of flight for radiation traveling from the rear surface to the probe. The associated polar plot suggests that this source will produce a ringlike radiation pattern.

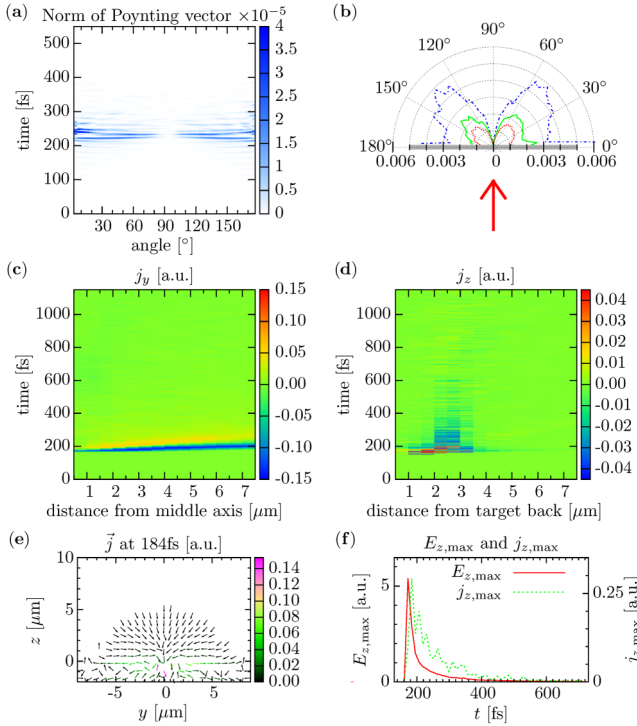


FIG. 4 (color online). (a) Time-traces of the angle-resolved norm of the Poynting vector recorded by the probes on a $20\ \mu\text{m}$ hemisphere behind the target. (b) Time-integrated polar plot of the radiation trace [shown in (a)] measured at three semicircles of radii $20\ \mu\text{m}$ (dotted red curve), $40\ \mu\text{m}$ (solid green curve), and $60\ \mu\text{m}$ (dashed blue curve), respectively. The target lies along 0° – 180° direction and the laser pulse is incident in the 270° – 90° (red arrow) direction. “Streak” image of current density (c) J_y component (along surface between 67.5 and $74.5\ \mu\text{m}$, laser is at $75\ \mu\text{m}$) and (d) J_z (perpendicular to the target). (e) Current density vectors at $184\ \text{fs}$. (f) Lineouts of maximum field E_z (solid curve) and current j_z (dashed curve) along the central rear target normal.

A second source of THz radiation associated with the time varying charge separation (TNSA) field [25,31] can also be identified. In this simulation, the field decays rapidly over around $200\ \text{fs}$ -Fig. 4(f), its peak moving outwards with a velocity $\approx 0.1c$ consistent with the measured proton energies. This dipolar electric field and its associated longitudinal current can be derived from Mora’s expansion model [31]. According to this model, the field (E_f) and the current (J_f) at the ion front decay as $\sim t^{-1}$ and $\sim t^{-2}$, respectively, whereas our simulations suggest a faster decay, $E_f \sim t^{-3}$ and a similar falloff for J_f . This is probably because of the short pulse length used in the simulation (as opposed to the constant irradiance assumed by the model), which limits the hot electron driving term, effectively leading to a rapid reduction in the hot electron density. The model also predicts that the current only depends on the hot electron temperature, providing a natural correlation to the proton numbers and cutoff energy. Radiation from this source is emitted radially, almost parallel to the target surface.

Longer-lived return currents triggered by this initial expansion could in principle lead to further emission at lower frequencies in the 0.1 – $30\ \text{THz}$ band. However, limited resolution and sampling of parameter space in the present simulations prevents direct quantitative comparison with the experiment here.

In summary, we report the observation of a compact and powerful gigawatt class T -ray source based on laser-driven ion acceleration. Subpicosecond duration T -ray pulses with energy up to $460\ \mu\text{J}$ in the 0.1 – $30\ \text{THz}$ band at $10\ \text{Hz}$ repetition rate were measured. Results of the spectral measurements with bandpass filters were comparable to the measurements with the electro-optic method. The peak power of our THz source of $0.8\ \text{GW}$ is thus even higher than that of state-of-the-art synchrotrons [32], while the average power of source is over $4\ \text{mW}$, only limited by the repetition rate of the laser system. In addition to a high conversion efficiency ($> 7 \times 10^{-4}$), a unique feature of our source lies in the possibility of simultaneously generating high energy THz pulses along with an energetic ion beam, a characteristic which could be exploited to develop future laser-driven particle acceleration schemes [33]. Analysis of 2D PIC simulations revealed the presence of fast decaying currents at the target rear surface, one component of which can be associated with the TNSA ion acceleration mechanism. Both experiment and modeling therefore suggest a strong and intriguing correlation between THz emission and rear-surface ion acceleration: further experimental investigation is clearly needed to fully quantify this relation.

A. G. acknowledges the support of Carl-Zeiss-Stiftung and Deutsche Forschungsgemeinschaft (DFG). The authors thank B. Beleites, F. Ronneberger, and O. Jaeckel for the smooth operation of the JETI laser. The authors are also grateful to B. Steffen and B. Schmidt from DESY Hamburg for fruitful discussions. A. K. and P. G. acknowledge support by the Alliance Program of the Helmholtz Association (HA216/EMMI) and computational resources awarded under Project No. JZAM04.

*Corresponding author.

amrutha.gopal@uni-jena.de

[†]Present address: Institut für Photonische Technologien, Postfach 100239, 07702 Jena, Germany.

[‡]Present address: Leibniz-Rechenzentrum, Boltzmannstr. 1, 85748 Garching, Germany.

- [1] M. Tonouchi, *Nat. Photonics* **1**, 97 (2007).
- [2] P. H. Siegel, *IEEE Trans. Microwave Theory Tech.* **52**, 2438 (2004).
- [3] J. F. Federici, B. Schulkin, F. Huang, D. Gary, R. Barat, F. Oliveira, and D. Zimdars, *Semicond. Sci. Technol.* **20**, S266 (2005).
- [4] B. E. Cole, J. B. Williams, B. T. King, M. S. Sherwin, and C. R. Stanley, *Nature (London)* **410**, 60 (2001).

- [5] M.C. Hoffmann and J.A. Fülöp, *J. Phys. D* **44**, 083001 (2011).
- [6] E. Berry, A.J. Fitzgerald, N.N. Zinovev, G.C. Walker, S. Homer-Vanniasinkam, C.D. Sudworth, R.E. Miles, J.M. Chamberlain, and M.A. Smith, *Proc. SPIE Int. Soc. Opt. Eng.* **5030**, 459 (2003).
- [7] W. Kuehn, K. Reimann, M. Woerner, and T. Elsaesser, *J. Chem. Phys.* **130**, 164503 (2009).
- [8] I. Tudosa, C. Stamm, A.B. Kashuba, F. King, H.C. Siegmann, J. Stöhr, G. Ju, B. Lu, and D. Weller, *Nature (London)* **428**, 831 (2004).
- [9] C.H. Back, D. Weller, J. Heidmann, D. Mauri, D. Guarisco, E. Garwin, and H. Siegmann, *Phys. Rev. Lett.* **81**, 3251 (1998).
- [10] S. Casalbuoni, B. Schmidt, P. Schmüser, V. Arsov, and S. Wesch, *Phys. Rev. ST Accel. Beams* **12**, 030705 (2009).
- [11] D.H. Auston, K. Cheung, J. Valdmanis, and D. Kleinman, *Phys. Rev. Lett.* **53**, 1555 (1984).
- [12] G.L. Carr, M.C. Martin, W.R. McKinney, K. Jordan, G.R. Neil, and G.P. Williams, *Nature (London)* **420**, 153 (2002).
- [13] A.G. Stepanov, L. Bonacina, S.V. Chekalin, and J.-P. Wolf, *Opt. Lett.* **33**, 2497 (2008).
- [14] V.B. Gildenburg and N. Vvedenskii, *Phys. Rev. Lett.* **98**, 245002 (2007).
- [15] V.A. Kostin and N.V. Vvedenskii, *Opt. Lett.* **35**, 247 (2010).
- [16] K. Y. Kim, A. J. Taylor, J. H. Glowia, and G. Rodriguez, *Nat. Photonics* **2**, 605 (2008).
- [17] H. Hamster, A. Sullivan, S. Gordon, W. White, and R. Falcone, *Phys. Rev. Lett.* **71**, 2725 (1993).
- [18] A. Sagisaka *et al.*, *Appl. Phys. B* **90**, 373 (2008).
- [19] C. Li *et al.*, *Phys. Rev. E* **84**, 036405 (2011).
- [20] W.P. Leemans *et al.*, *Phys. Rev. Lett.* **91**, 074802 (2003).
- [21] S.L. Chin *et al.*, *Laser Phys.* **22**, 1 (2012).
- [22] W.M. Wang, Z.-M. Sheng, H.-C. Wu, M. Chen, C. Li, J. Zhang, and K. Mima, *Opt. Express* **16**, 16999 (2008).
- [23] A. Gopal *et al.*, *New J. Phys.* **14**, 083012 (2012).
- [24] H. Schwoerer, S. Pfotenhauer, O. Jäckel, K.-U. Amthor, B. Liesfeld, W. Ziegler, R. Sauerbrey, K. W. D. Ledingham, and T. Esirkepov, *Nature (London)* **439**, 445 (2006).
- [25] S.C. Wilks, A.B. Langdon, T.E. Cowan, M. Roth, M. Singh, S. Hatchett, M.H. Key, D. Pennington, A. MacKinnon, and R.A. Snavely, *Phys. Plasmas* **8**, 542 (2001).
- [26] J. Shan, A. S. Weling, E. Knoesel, L. Bartels, M. Bonn, A. Nahata, G.A. Reider, and T.F. Heinz, *Opt. Lett.* **25**, 426 (2000).
- [27] J. D. Jackson, *Classical Electrodynamics* (Wiley, New York, 1999), Chap. 14, 3rd ed.
- [28] J. Fuchs, *et al.*, *Nat. Phys.* **2**, 48 (2006).
- [29] JUSPIC, Jülich (Super-) Scaling Particle-In-Cell code, <http://www.fz-juelich.de/ias/jsc/jusplic>.
- [30] See Supplemental Material at <http://link.aps.org/supplemental/10.1103/PhysRevLett.111.074802> for details.
- [31] P. Mora, *Phys. Rev. Lett.* **90**, 185002 (2003).
- [32] J.H. Booske, R.J. Dobbs, C.D. Joye, C.L. Kory, G.R. Neil, G.-S. Park, J. Park, and R.J. Temkin, *IEEE Trans. Terahertz Sci. Technol.* **1**, 54 (2011).
- [33] R.B. Palmer, *Part. Accel.* **11**, 81 (1980).